AGU PUBLICATIONS

JGR

Journal of Geophysical Research: Atmospheres

RESEARCH ARTICLE
10.1002/2017JD026874

Special Section:
Simulations of stratospheric sulfate aerosol geoengineering with the Whole Atmosphere Community Climate Model (WACCM)

This article is a companion to Mills et al. (2017), https://doi.org/10.1002/2017JD027006; Richter et al. (2017), https://doi.org/10.1002/2017JD026912; MacMartin et al. (2017), https://doi.org/10.1002/2017JD026868; and Tilmes et al. (2017), https://doi.org/10.1002/2017JD026888

Key Points:
- We present the first simulations of stratospheric aerosol geoengineering using multiple injection locations
- Three simultaneous temperature objectives were successfully met
- There are residuals/side effects, which may or may not represent potential objectives that could be met by geoengineering

Supporting Information:
- Supporting Information S1

Correspondence to:
B. Kravitz,
ben.kravitz@pnnl.gov

Citation:
Kravitz, B., MacMartin, D. G., Mills, M. J., Richter, J. H., Tilmes, S., Lamarque, J.-F., … Vitt, F. (2017). First simulations of designing stratospheric sulfate aerosol geoengineering to meet multiple simultaneous climate objectives. *Journal of Geophysical Research: Atmospheres*, *122*, 12,616–12,634. https://doi.org/10.1002/2017JD026874

Received 30 MAR 2017
Accepted 12 OCT 2017
Accepted article online 6 NOV 2017
Published online 7 DEC 2017

First Simulations of Designing Stratospheric Sulfate Aerosol Geoengineering to Meet Multiple Simultaneous Climate Objectives

Ben Kravitz[1], Douglas G. MacMartin[2,3], Michael J. Mills[4], Jadwiga H. Richter[5], Simone Tilmes[4,5], Jean-Francois Lamarque[4], Joseph J. Tribbia[5], and Francis Vitt[4]

[1] Atmospheric Sciences and Global Change Division, Pacific Northwest National Laboratory, Richland, WA, USA, [2] Mechanical and Aerospace Engineering, Cornell University, Ithaca, NY, USA, [3] Department of Computing and Mathematical Sciences, California Institute of Technology, Pasadena, CA, USA, [4] Atmospheric Chemistry, Observations, and Modeling Laboratory, National Center for Atmospheric Research, Boulder, CO, USA, [5] Climate and Global Dynamics Laboratory, National Center for Atmospheric Research, Boulder, CO, USA

Abstract We describe the first simulations of stratospheric sulfate aerosol geoengineering using multiple injection locations to meet multiple simultaneous surface temperature objectives. Simulations were performed using CESM1(WACCM), a coupled atmosphere-ocean general circulation model with fully interactive stratospheric chemistry, dynamics (including an internally generated quasi-biennial oscillation), and a sophisticated treatment of sulfate aerosol formation, microphysical growth, and deposition. The objectives are defined as maintaining three temperature features at their 2020 levels against a background of the RCP8.5 scenario over the period 2020–2099. These objectives are met using a feedback mechanism in which the rate of sulfur dioxide injection at each of the four locations is adjusted independently every year of simulation. Even in the presence of uncertainties, nonlinearities, and variability, the objectives are met, predominantly by SO_2 injection at 30°N and 30°S. By the last year of simulation, the feedback algorithm calls for a total injection rate of 51 Tg SO_2 per year. The injections are not in the tropics, which results in a greater degree of linearity of the surface climate response with injection amount than has been found in many previous studies using injection at the equator. Because the objectives are defined in terms of annual mean temperature, the required geongineering results in "overcooling" during summer and "undercooling" during winter. The hydrological cycle is also suppressed as compared to the reference values corresponding to the year 2020. The demonstration we describe in this study is an important step toward understanding what geoengineering can do and what it cannot do.

Plain Language Summary Understanding what geoengineering can and cannot do is crucial for narrowing uncertainties in the range of potential responses to future climate change. Part of this effort is to demonstrate the capability of meeting specified climate objectives in a climate model in the presence of uncertainty in climate response. Here we provide the first demonstration of a strategy for meeting three simultaneous global temperature objectives via stratospheric sulfate aerosol geoengineering, using a state-of-the-art climate model that represents key processes relevant to the potential climate responses. We show that the objectives can be met successfully using an algorithm we have developed, and we also demonstrate some potential side effects, which could be potential objectives for which we did not control.

1. Introduction

Geoengineering, or the deliberate modification of the climate system to offset the effects of global warming, has received increasing amounts of attention (e.g., Crutzen, 2006; National Research Council (NRC), 2015). One of the most commonly discussed methods is stratospheric sulfate aerosol geoengineering, involving large, regular injections of sulfate aerosol precursors (often SO_2) into the stratosphere (e.g., Budyko, 1974). This aims at mimicking the aerosol layer created by large volcanic eruptions, which is known to cause global cooling (e.g., Robock, 2000). If geoengineering is to be considered as a potential response to addressing climate change, its effects, potentials, and limitations need to be quantified, particularly in comparison

to other methods of addressing climate change, including mitigation of greenhouse gas emissions, adaptation to climate change, or carbon dioxide removal (e.g., MacMartin et al., 2016; Tilmes et al., 2016). Put simply, society needs to know what geoengineering can do and what it cannot do.

Many past studies, particularly those under the Geoengineering Model Intercomparison Project (GeoMIP) (Kravitz et al., 2011), have implicitly focused on the question, "What will happen to the climate under geoengineering?" This sort of approach has been quite useful in understanding the climate effects that result from simulating geoengineering in specific ways, including the effects on mean climate, the hydrological cycle, the cryosphere, extreme events, stratospheric chemistry, and the land biosphere (e.g., Berdahl et al., 2014; Curry et al., 2014; Glienke et al., 2015; Kravitz et al., 2013; Moore et al., 2014; Pitari et al., 2014; Tilmes et al., 2013; Xia et al., 2014). However, by adding tools and perspectives from engineering, we can expand the scope of geoengineering studies to include the question, "Can geoengineering be used to achieve specific climate objectives?"

Independent of choosing which climate objectives are most important for geoengineering to meet, a task that we are not qualified to undertake, this question belies the need for a *design* perspective to geoengineering approaches. For example, when considering stratospheric sulfate aerosol geoengineering, the resulting climate effects depend upon the altitude of injection, latitude of injection, how much is injected, and what time of year (Kravitz, 2013; Tilmes et al., 2017). There is some ability to tailor geoengineering to produce particular desired effects, although there are necessarily limitations; that is, geoengineering likely cannot be used to achieve any arbitrary set of climate objectives. We also note that since designing a geoengineering strategy will inevitably involve using climate models, this ability to tailor the effects is predicated on the assumption that climate models sufficiently represent the system dynamics of the real world.

This design perspective has been explored in idealized cases in the past. Ban-Weiss and Caldeira (2010) and MacMartin et al. (2013) explored optimization of different potential objectives by assessing the climate response to different spatiotemporal patterns of solar reduction. Uniform solar reduction has been shown to approximate the broad global and latitudinal radiative and surface climate effects of stratospheric sulfate aerosol injection in the tropics (Kalidindi et al., 2014; Niemeier et al., 2013), although disparities do emerge when evaluating regional changes or changes at finer scale than broad global features (e.g., Ferraro et al., 2015a). MacMartin, Kravitz, et al. (2014) were the first to demonstrate how one can use feedback (described in more detail later) to regularly modify the amount of solar irradiance reduction to meet chosen global mean temperature objectives in a climate model in the presence of uncertainty. Kravitz et al. (2014) expanded upon this study by demonstrating that, for this particular feedback algorithm, the same objective could be met with the same algorithm in an entirely different model; although such a demonstration does not fully represent the challenge of bridging the gap between models and reality, it is a necessary step in establishing robustness to uncertainty. Kravitz et al. (2016) then demonstrated, again in two distinct climate models, that if one changes solar irradiance in latitude-dependent patterns (MacMartin et al., 2013), one can use feedback to meet multiple simultaneous climate objectives in the presence of uncertainty.

These previous studies made crucial steps toward the overall objective of understanding what geoengineering can do and what it cannot do. However, with one exception (Jackson et al., 2015), all of these studies using feedback, including modifications of both single and multiple degrees of freedom, involved changes in solar irradiance. Although this is a good approximation of many large-scale features of stratospheric sulfate aerosol geoengineering, there are some crucial differences that ultimately limit the utility of this approach. One difference involves atmospheric circulation and transport of the injected aerosols, which is to a large degree uncontrollable, so there is no way to guarantee that one can use stratospheric aerosols to achieve the same pattern of radiative forcing that was imposed by solar irradiance reduction. Second, one of the key sources of uncertainty and nonlinearity in stratospheric sulfate aerosols is aerosol microphysical growth. Depending on the amount of total injection required, the resulting radiative forcing for each incremental increase in injection amount can be highly sublinear (Niemeier & Timmreck, 2015). Moreover, the resulting stratospheric heating from the aerosols and effects on ozone chemistry (e.g., Ferraro et al., 2011; Pitari et al., 2014; Richter et al., 2017; Tilmes et al., 2009, 2017), aerosol-cloud interactions as the stratospheric sulfate aerosols fall into the troposphere, and the resulting climate effects of all of these all depend upon aerosol size. These effects cannot be captured by solar irradiance reduction. We note that many of these processes (e.g., tropospheric and stratospheric dynamical responses to stratospheric heating and the resulting effects on surface climate)

are poorly constrained and are likely a significant source of uncertainty and intermodel variability in any simulation involving stratospheric sulfate aerosols (MacMartin et al., 2016).

Here we provide the first demonstration of the ability to meet multiple simultaneous climate objectives in the presence of uncertainty with stratospheric sulfate aerosol geoengineering using a state-of-the-art climate model. This manuscript is accompanied by several others (Mills et al., 2017; Richter et al., 2017; Tilmes et al., 2017; MacMartin et al., 2017) that have described many of the details that led to the ability to reach this point; we repeat the salient points from those manuscripts as necessary.

In section 2, we describe the study we conducted, including the objectives and the feedback algorithm. In section 3, we describe the results of the simulations we conducted. In section 4, we discuss some of the finer points of our simulations, highlighting some potential areas for improvement. In section 5, we summarize our study and provide conclusions.

2. Methodology

Kravitz et al. (2016) outlined four key steps in demonstrating the ability of geoengineering to meet particular climate objectives:

1. An explicit definition of the specific objectives of geoengineering;
2. Determination of the particular degrees of freedom to be modified to meet the objectives;
3. A strategy for meeting the objectives in the presence of uncertainty;
4. Verification of the designed strategy in a different evaluation model.

In subsequent sections, we describe each of the steps as they apply to the present study.

All of the simulations described in this manuscript were conducted with a version of the Community Earth System Model Version 1(CESM; Hurrell et al., 2013) that involves fully coupled atmosphere, ocean, sea ice, land ice, and dynamic land vegetation models. The particular iteration of this model is CESM1(WACCM) with CAM5 physics. More specifically, the atmosphere is a version of the Whole Atmosphere Community Climate Model (WACCM; Marsh et al., 2013; Mills et al., 2016) that has been modified to have a horizontal resolution of 1° and has an internally generated quasi-biennial oscillation. The features of CESM1(WACCM), which are described in more detail by Mills et al. (2017), include a full tropospheric and stratospheric sulfate aerosol treatment (conversion of SO_2 into sulfate aerosols, microphysical growth including coalescence and condensation processes, and sedimentation) that is fully interactive with both radiative heating and dynamical transport. These processes are crucial to proper representation of stratospheric sulfate aerosol geoengineering, as this ensures that some of the key uncertainties and nonlinearities involved with stratospheric sulfate aerosols are included. Mills et al. (2016) and Mills et al. (2017) have validated this model against aerosol optical depth data from the 1991 eruption of Mount Pinatubo, showing the model's excellent performance.

2.1. Objectives

We choose the same objectives as were chosen by Kravitz et al. (2016) (Figure 1). Against a background corresponding to the RCP8.5 scenario (Meinshausen et al., 2011; Moss et al., 2010) over the period 2020–2099, we use stratospheric sulfate aerosol geoengineering (injection of SO_2 into the stratosphere) to maintain global mean surface temperature (T_0), the interhemispheric surface temperature gradient (T_1), and the equator-to-pole surface temperature gradient (T_2) at their 2020 values according to the RCP8.5 simulation (also called the *reference* simulation). More specifically, we define

$$\begin{aligned} T_0 &= \frac{1}{A}\int_{-\pi/2}^{\pi/2} T(\psi)\,\mathrm{d}A \\ T_1 &= \frac{1}{A}\int_{-\pi/2}^{\pi/2} T(\psi)\sin\psi\,\mathrm{d}A \\ T_2 &= \frac{1}{A}\int_{-\pi/2}^{\pi/2} T(\psi)\frac{1}{2}(3\sin^2\psi - 1)\,\mathrm{d}A \end{aligned} \tag{1}$$

where $\mathrm{d}A = \cos(\psi)\mathrm{d}\psi$ describes the area of a latitude band, and $A = 2\pi R_E^2 \int_{\psi=-\pi/2}^{\psi=\pi/2} \mathrm{d}A$ is the total surface area of the Earth integrated over latitude bands $\mathrm{d}A$ (R_E is Earth's radius). The reference values for each of these

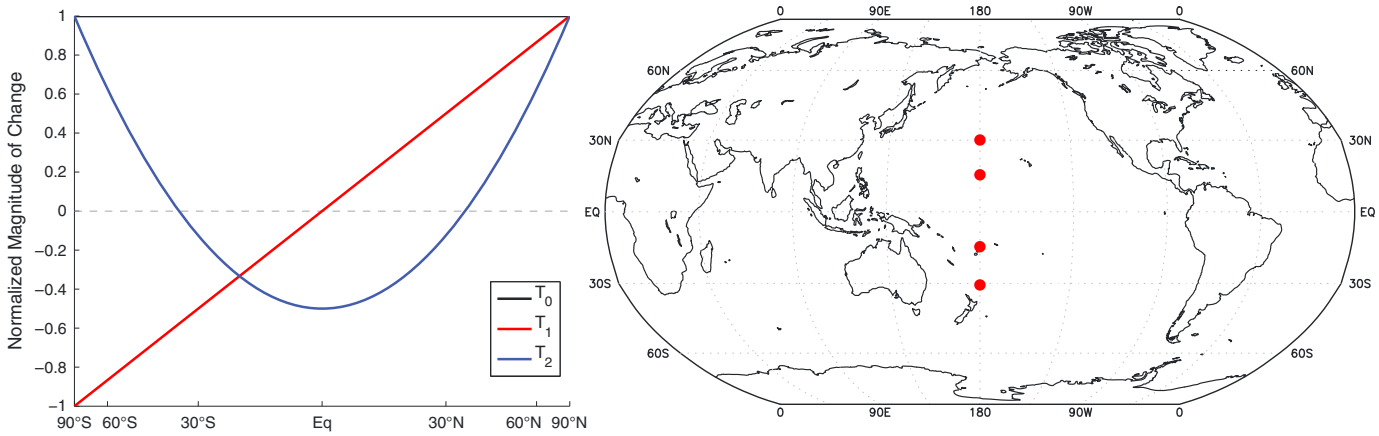

Figure 1. The three temperature objectives (T_0, T_1, and T_2; (left) Equation (1) relative to 2020 as a function of latitude and (right) the four SO_2 injection locations. All values in Figure 1 (left) are normalized so that the value 1 indicates the largest magnitude of temperature reduction.

objectives, obtained by averaging an RCP8.5 simulation carried out with the same model over the period 2015–2024 are (in Kelvin)

$$T_0^{\text{ref}} = 288.13$$
$$T_1^{\text{ref}} = 0.76$$
$$T_2^{\text{ref}} = -5.98$$

These three objectives were chosen to be consistent with many previously noted results from solar irradiance reduction simulations and, to some extent, simulations with stratospheric sulfate aerosols (e.g., Kravitz et al., 2013; Robock et al., 2008). CO_2-induced warming has a number of features, but we point out three major patterns: global warming (an increase in T_0), more warming in the Northern Hemisphere than in the Southern Hemisphere (an increase in T_1), and polar amplification of warming relative to lower latitudes (an increase in T_2). Geoengineering via total solar irradiance reduction or tropical injection of stratospheric sulfate aerosols is effective at cooling the globe (T_0), but it tends to cool the Northern Hemisphere more than the Southern Hemisphere, changing T_1 in different ways than CO_2-induced changes in T_1, which can lead to shifts in precipitation patterns (Haywood et al., 2016). It also is less effective at offsetting the changes in T_2 caused by CO_2-induced warming, leaving residual polar warming. As such, deliberately targeting all three broad temperature objectives (T_0, T_1, and T_2) will help avoid some of these known side effects that were revealed in many past simulations of geoengineering.

2.2. Degrees of Freedom

Determining the appropriate degrees of freedom (what to modify in the climate system to successfully meet the chosen objectives) is not a simple process. This effort, also called *system identification*, began with the simulations described by Tilmes et al. (2017), in which the injection parameter space was coarsely sampled via 10 year simulations involving different amounts of stratospheric SO_2 injection at different latitudes and altitudes. Tilmes et al. (2017) discuss the results from these simulations in greater detail, and MacMartin et al. (2017) discuss the linearity of these simulations and the ultimate selection of the degrees of freedom to be modified.

The end result of this selection process is four chosen degrees of freedom: the amount of SO_2 injected at each of the four independent locations (Figure 1). More specifically, these locations are at 30°S, 15°S, 15°N, and 30°N in latitude along 180° longitude at high altitude (approximately 5 km above the annual mean tropopause). MacMartin et al. (2017) discuss the details of why these four locations were chosen, but roughly summarizing, different combinations of injection in these four locations are capable of producing patterns of aerosol optical depth (AOD) that are constant (ℓ_0), linear (ℓ_1), and quadratic (ℓ_2) with latitude. These three patterns

are defined analogously to the definitions in equation (1), but with a different normalization so that at any latitude ψ, $\mathrm{AOD}(\psi) = \ell_0 + \ell_1 \sin(\psi) + \ell_2(3\sin^2(\psi) - 1)/2$:

$$\begin{aligned}\ell_0 &= \frac{\xi_0}{A}\int_{-\pi/2}^{\pi/2} \mathrm{AOD}(\psi)\,\mathrm{d}A \\ \ell_1 &= \frac{\xi_1}{A}\int_{-\pi/2}^{\pi/2} \mathrm{AOD}(\psi)\sin\psi\,\mathrm{d}A \\ \ell_2 &= \frac{\xi_2}{A}\int_{-\pi/2}^{\pi/2} \mathrm{AOD}(\psi)\frac{1}{2}(3\sin^2\psi - 1)\,\mathrm{d}A\end{aligned} \tag{2}$$

where AOD is zonally averaged stratospheric sulfate aerosol optical depth. In turn, MacMartin et al. (2017) demonstrate that these three patterns of AOD can produce somewhat controllable changes in T_0, T_1, and T_2. The normalization factors are defined as

$$\begin{aligned}\xi_0 &= \frac{1}{2}\int_{-\pi/2}^{\pi/2} \mathrm{d}A = 1 \\ \xi_1 &= \frac{1}{2}\int_{-\pi/2}^{\pi/2} \sin^2(\psi)\mathrm{d}A = \frac{1}{3} \\ \xi_2 &= \frac{1}{2}\int_{-\pi/2}^{\pi/2} \left(\frac{3\sin^2(\psi) - 1}{2}\right)^2 \mathrm{d}A = \frac{1}{5}\end{aligned} \tag{3}$$

In principle, one could define $\{\ell_i\}$ exactly the same as $\{T_i\}$ and renormalize the control gains (defined in the subsequent section) to account for these differences. For the easiest comparability with Kravitz et al. (2016), both in terms of the objectives $\{T_i\}$ and the control gains, we have opted to include the normalization here in the definitions of $\{\ell_i\}$.

We stress that this effort is, to a large extent, an illustration of capability, and we did not sufficiently sample the aerosol injection parameter space to fully ascertain the potentials and limitations of stratospheric sulfate aerosol geoengineering. Doing so would require simulations at a greater number of latitudes, altitudes, and magnitudes than Tilmes et al. (2017) describe, and one would also need more thorough tests of linearity than what MacMartin et al. (2017) elucidate. Moreover, one would need to understand the effects of injection at different times of year, which is a degree of freedom not explored here. Additionally, as we will demonstrate later, 10 years is insufficient to properly characterize the system dynamics on all time scales of interest. Although the feedback algorithm (described in the next section) was capable of compensating for uncertainties introduced by this coarse sampling of the frequency space, such performance is not guaranteed for all possible sets of objectives. Finally, if the purpose is to truly explore the parameter space for the purpose of supporting decisions regarding deployment of geoengineering, one would want to more thoroughly sample the space of intermodel variations. Even with unlimited computational resources, simulations with a single model are only capable of characterizing system dynamics of that model.

2.3. Feedback Algorithm

Once the objectives and degrees of freedom are established, the next step is to design a strategy to meet the objectives by modifying the degrees of freedom (in this case, the injection amount at each of the four latitudes), all in the presence of uncertainty in the climate response to greenhouse gases and stratospheric sulfate aerosol geoengineering, as well as uncertainty introduced by natural climate variability. Much of this section is rather detailed, so readers can skip to section 3 if they are not interested in how to construct the strategy used here.

Designing a strategy requires sufficient characterization of the dynamics of the input-output relationships in the system (how modifying the degrees of freedom affects the chosen objectives), a process called *system identification*. Kravitz et al. (2016) describe multiple methods of obtaining these relationships. For the present study, we found that the simulations described by Tilmes et al. (2017) and MacMartin et al. (2017) provided sufficient information to design a strategy that could meet the chosen objectives. This conclusion allowed us to avoid the computational expense associated with additional system identification simulations.

Kravitz et al. (2016) were able to design their strategy in a relatively straightforward manner, as the connection between solar reduction and surface temperature is clear. Here the procedure is slightly more complicated,

Table 1
Magnitudes of the Transfer Function (Influence Matrix) G Relating T (Temperature; Rows) and ℓ (Aerosol Optical Depth; Columns), Projected Onto Constant, Linear, and Quadratic Functions of Latitude (Equation (1))

	ℓ_0	ℓ_1^S	ℓ_1^N	ℓ_2
T_0	**−5.2637**	*−0.4897*	*0.4241*	*−0.1312*
T_1	−1.2318	**−1.5220**	**1.5002**	*−0.0435*
T_2	−0.4938	−0.4183	0.2765	**−0.2836**

Note. Boldface values denote the diagonal components of the matrix. Italic values denote off-diagonal components of the matrix that represent weak (negligible) influences of AOD on temperature. The influence matrix is lower triangular dominant.

as SO_2 injection is first transported and converted to aerosols, and those aerosols then exert a radiative forcing that causes surface temperature change. MacMartin et al. (2017) derive these relationships, which we repeat here.

We first note that the different injection locations will affect the patterns ℓ_0, ℓ_1, and ℓ_2 of AOD differently. More specifically, repeating the results of MacMartin et al. (2017),

1. Injection at 15°S and 15°N affects ℓ_0.
2. Injection at 15°N and 30°N or injection at 15°S and 30°S primarily affects $\ell_1 \pm \ell_0$.
3. Injection at 30°N and 30°S primarily affects $\ell_2 + \ell_0$.

This allows us to form part of an influence matrix, whereby we know which injection locations affect which spatial patterns of AOD. Second, based on the simulations described by Tilmes et al. (2017) and MacMartin et al. (2017), we can identify the approximate magnitude of injection that will result in unit AOD for each of ℓ_0, ℓ_1, and ℓ_2. Assembling these values, we can then form a matrix relating SO_2 injection amounts at four locations (q) to spatial patterns of aerosol optical depth (ℓ):

$$\begin{bmatrix} q_{30S} \\ q_{15S} \\ q_{15N} \\ q_{30N} \end{bmatrix} = \begin{bmatrix} 20\ell_1^S + 40\ell_2 \\ 30\left(\ell_0 - \left(\ell_1^N + \ell_1^S + \ell_2\right)\right) + 45\ell_1^S \\ 30\left(\ell_0 - \left(\ell_1^N + \ell_1^S + \ell_2\right)\right) + 45\ell_1^N \\ 20\ell_1^N + 40\ell_2 \end{bmatrix} \tag{4}$$

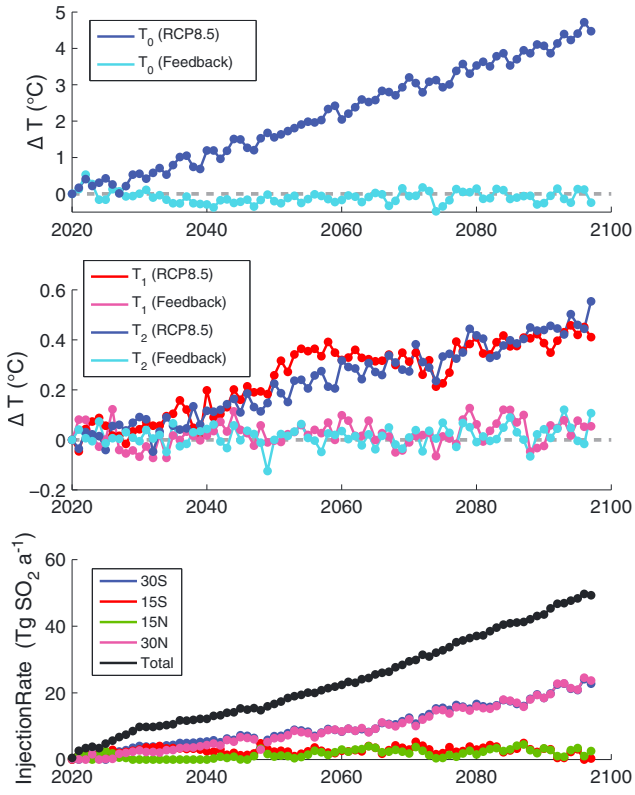

Figure 2. Illustration of the performance of the feedback algorithm (as compared to the ungeoengineered RCP8.5 simulation) in meeting the chosen temperature objectives (grey dashed lines). All circles indicate annually averaged values. (top and middle) The different temperature quantities defined in Section 2.1 and (bottom) the required injection at each latitude to meet those objectives. Change is measured from the year 2020 average.

where the projection ℓ_1 is separated into northward and southward components defined by $\ell_1^N = \max(\ell_1, 0)$ and $\ell_1^S = -\min(\ell_1, 0)$. This ensures that all entries in the vector $\vec{\ell}$ are nonnegative. We then impose two constraints to ensure that all injection amounts are positive. The first is that $\ell_0 \geq |\ell_1|$. After that constraint is satisfied, the second constraint is that $\ell_0 \geq |\ell_1| + \ell_2$. If these constraints are violated, then $|\ell_1|$ or ℓ_2 are reduced accordingly.

The second step relates $\vec{\ell}$ with the temperature objectives T_0, T_1, and T_2 (described above). We denote this relationship as G. MacMartin et al. (2017) estimate the magnitudes of the relationships in the matrix G; these magnitudes are repeated in Table 1. We note that G is lower triangular dominant; that is, perturbations to ℓ_0 affect all three temperature objectives, perturbations to ℓ_1 primarily affect T_1 and T_2, and perturbations to ℓ_2 primarily affect T_2.

In designing a strategy, we can first use the sensitivities in G to estimate our best guess as to how much aerosol optical depth is required to meet the objectives in any given year. This is called a *feedforward*. From the RCP8.5 simulation, T_0 changes by approximately 0.0595°C per year. Per the matrix in Table 1, T_0 decreases by approximately 5.26°C per unit of AOD. Therefore, we predict that ℓ_0 will need to increase by approximately $\frac{0.0595}{5.26} = 0.011$ per year to account for the increase in T_0 under RCP8.5. As such, we define the first term in the feedforward to be $\hat{\ell}_0 = 0.011(t - t_{\text{ref}})$ where t_{ref} is the base year for simulation (2020), and t is any year of simulation.

To calculate the feedforward for ℓ_1, we need information about both the required change in ℓ_1 to offset a given change in T_1, as well as the off-diagonal terms (how much changes in ℓ_0 affect T_1). We compute the feedforward $\hat{\ell}_1 = \left[\frac{0.0056}{1.52} - 0.011 \cdot \frac{1.23}{1.52}\right](t - t_{\text{ref}}) = -0.005(t - t_{\text{ref}})$. Similarly, $\hat{\ell}_2 = \left[\frac{0.0065}{0.28} + 0.005 \cdot \frac{0.42}{0.28} - 0.011 \cdot \frac{0.49}{0.28}\right](t - t_{\text{ref}}) = 0.0102(t - t_{\text{ref}})$. We then adjust the feedforward for ℓ_2 to account for the constraint

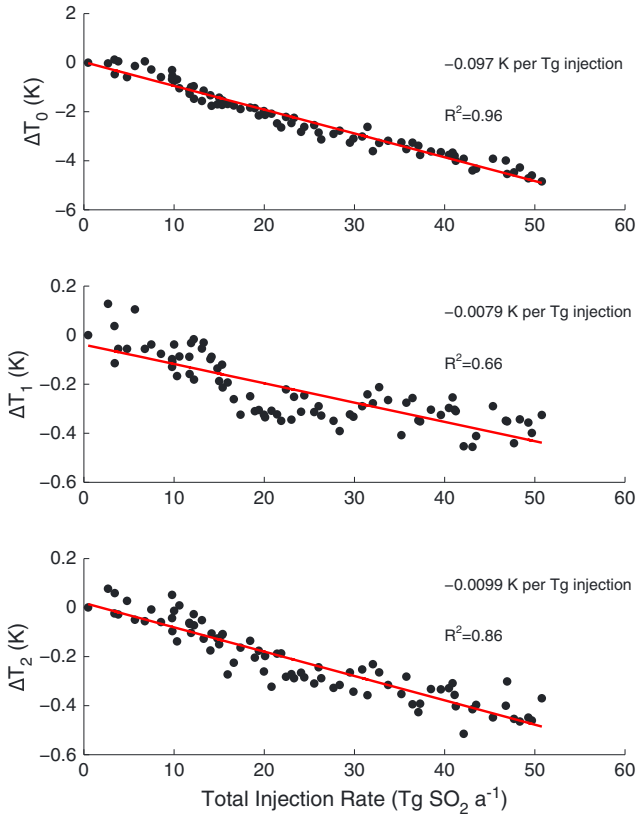

Figure 3. Comparison between total injection amount (black line in Figure 2) and annual mean temperature change (difference between temperature in RCP8.5 and the feedback run) for all three temperature objectives. Red lines indicate ordinary least squares regression through the black points.

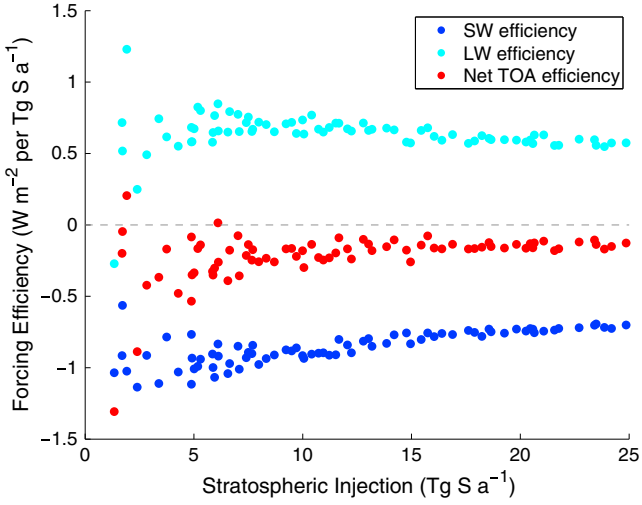

Figure 4. Forcing efficiency as a function of injection amount. Forcing efficiency is defined as the TOA radiative flux perturbation for a given injection rate in the feedback run. SW describes shortwave, LW describes longwave, and net describes SW + LW. All injection rates are in Tg S, following Niemeier and Timmreck (2015). All fluxes are defined as positive downward. Each dot indicates an annual average.

$\ell_0 \geq |\ell_1| + \ell_2$. (The other constraint of $\ell_0 \geq |\ell_1|$ is already met.) The quantity $\ell_0 - |\ell_1| - \ell_2 = -0.0039$, so we reduce the feedforward for ℓ_2 by that residual amount, such that $\hat{\ell}_2 = 0.006$.

We note that while designing this particular feedforward was relatively straightforward, it is overly simplistic and has a number of limitations. Specifically, it does not account for nonlinearities or different time constants in the response to AOD. An improved feedforward could be accomplished using a dynamic model instead of a linear fit, as was done by MacMartin, Caldeira, et al. (2014).

In practice, as was demonstrated by Kravitz et al. (2014), it is virtually impossible to accurately predict the required time series of AOD that will meet the objectives, because there are irreducible uncertainties in the climate response to radiative forcing. This is particularly true if there are nonlinearities in the system, which other studies have shown to be true for stratospheric sulfate aerosol geoengineering (MacMartin et al., 2017; Tilmes et al., 2017; Richter et al., 2017). To *manage* these uncertainties, we employ a feedback algorithm in which the SO_2 injection rate is updated at regular intervals (here yearly) based on how "close" the model state is to the chosen objectives. In a simple illustration, if the climate is too warm as compared to the chosen objective, more sulfate aerosol is added to the stratosphere (cooling the planet), and if the climate is too cold as compared to the chosen objective, the injection rate is reduced. We note that this is done regardless of the reason for the temperature difference from the objective: the feedback algorithm responds to any potential over or under geoengineering as well as natural variability (MacMartin, Kravitz, et al., 2014). The process of designing such a feedback algorithm has been described in detail by MacMartin, Kravitz, et al. (2014) and Kravitz et al. (2016), so many of the details will be omitted here.

As was done for solar reduction (Kravitz et al., 2016; MacMartin, Kravitz, et al., 2014), we choose a proportional integral control algorithm:

$$\ell_{i,j+1} = k_p(T_{i,j} - T_{i_{\mathrm{ref}}}) + k_i \sum_{q=1}^{j}(T_{i,q} - T_{i_{\mathrm{ref}}}) \quad (5)$$

where i denotes the component of the vectors ℓ or T (note that we are describing a single-variable case for ease of explanation), j describes the year of simulation that was just completed, $j+1$ describes the year of simulation that is about to be undertaken, and "ref" indicates the reference values given in equation (1) above. The k_p and k_i are the proportional and integral control gains, respectively, which describe how responsive the feedback algorithm is to deviations from the reference values. As in previous studies, we chose the *update rate* (how often the injection amounts are adjusted) to be 1 year. In principle, objectives could be chosen that require a subannual update rate, but that is beyond the scope of the present study.

We note that the feedforward is employed first, and then the feedback operates on the residual. This has the effect of taking some of the load off the feedback, in that it needs to act on much smaller deviations from the target. This has two advantages. One is that if the deviations are smaller, the margins for stability are greater, so one can use lower control gains while having the same overall performance (MacMartin, Kravitz, et al., 2014). This is particularly advantageous if there are errors in estimating the system dynamics. A second advantage is that because the deviations are smaller, there is less risk of nonlinearities affecting convergence of the feedback algorithm.

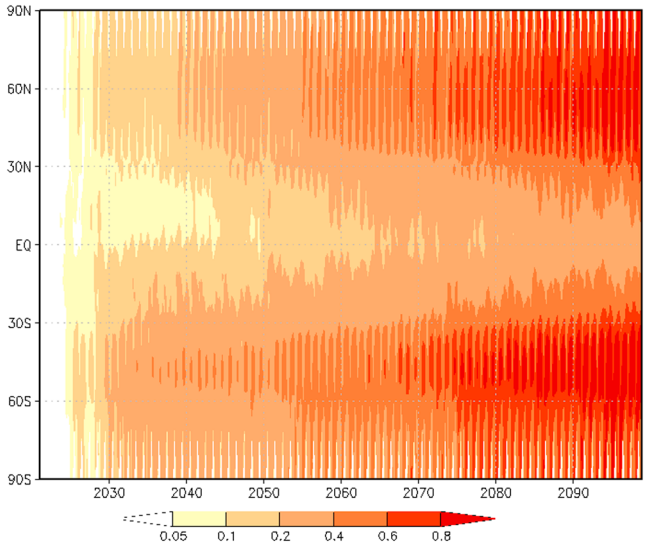

Figure 5. Zonally averaged monthly mean sulfate aerosol optical depth (AOD) in the feedback simulation. Note that AOD is not defined when there is no sunlight, hence, the zero values during polar night.

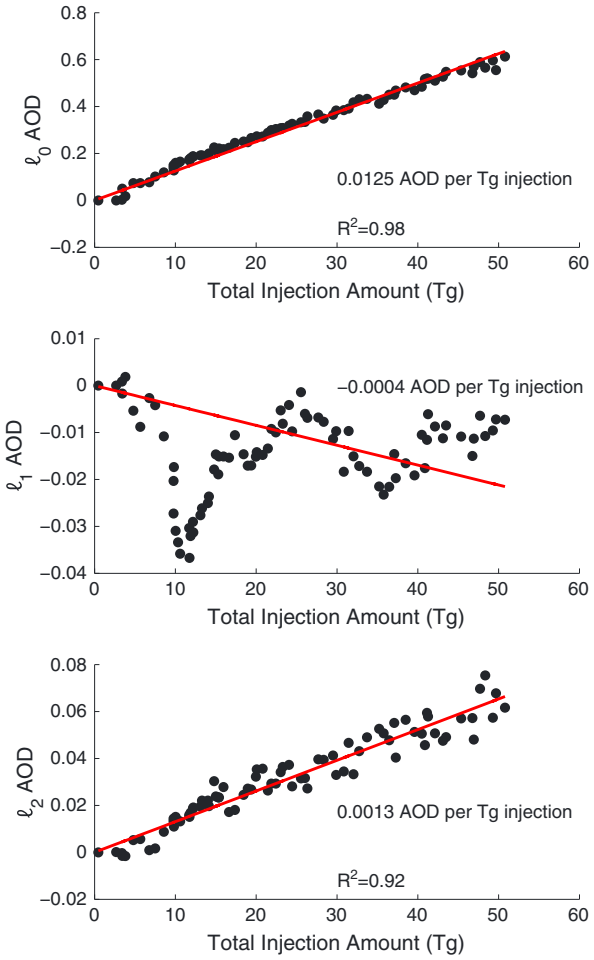

Figure 6. Comparison between total injection amount (black line in Figure 2) and the three projections of sulfate aerosol optical depth (ℓ_0, ℓ_1, and ℓ_2). Red lines indicate ordinary least squares regression through the black points, constrained to pass through the origin.

Kravitz et al. (2016) described the process of achieving these same three temperature objectives using solar reduction with the same three patterns as ℓ_0, ℓ_1, and ℓ_2. Therefore, we can use their estimates of control gains to inform our feedback algorithm. A 1% change in solar forcing exerts a global radiative forcing of approximately $-0.01 \cdot (1, 365/4) \cdot 0.7 = -2.39$ W m^{-2}. The global radiative forcing from one unit of stratospheric aerosol optical depth is approximately -23 W m^{-2} (Hansen et al., 1997). The ratio of these two represents approximately a factor of 10 difference, so taking one tenth of the control gains provided by Kravitz et al. (2016) should yield the approximately correct control gain values for the same time constant of response (here 5 years). As such, the feedback algorithm used here is

$$\Delta\ell_0 = 0.028\int_0^t (T_0 - T_{0_{\mathrm{ref}}})\,\mathrm{d}\tau + 0.028\,(T_0 - T_{0_{\mathrm{ref}}}) \tag{6}$$

$$\Delta\ell_1 = -0.75\Delta\ell_0 + 0.13\int_0^t (T_1 - T_{1_{\mathrm{ref}}})\,\mathrm{d}\tau + 0.13\,(T_1 - T_{1_{\mathrm{ref}}}) \tag{7}$$

$$\Delta\ell_2 = -\Delta\ell_1 - \Delta\ell_0 + 0.39\int_0^t (T_2 - T_{2_{\mathrm{ref}}})\,\mathrm{d}\tau + 0.39\,(T_2 - T_{2_{\mathrm{ref}}}). \tag{8}$$

where at the risk of abuse of notation, integrals are used instead of sums to more truthfully represent the concept of proportional integral control. The factors $-0.75\Delta\ell_0$ in the equation for $\Delta\ell_1$ and $-\Delta\ell_1 - \Delta\ell_0$ in the equation for $\Delta\ell_2$ are to account for the off-diagonal influences in the matrix *G*. (These off-diagonal factors were derived from a process called sequential loop closure. Kravitz et al. (2016) provide further details on the mathematics of this process.)

In any feedback system, an increase in the values of the overall gain will shorten the response time at the expense of making the system less stable. The overall gain is the product of the control gains and the system gain, the latter of which describes how responsive the system is to any perturbation. There are several potential sources of nonlinearity in this system that are responsible for changes in the system gain. One of them is aerosol coagulation: as the injection rate increases, there is increased coagulation onto existing aerosols, an increase in aerosol size, and hence a decrease in radiative forcing per unit injection (e.g., Heckendorn et al., 2009; Niemeier & Timmreck, 2015). Because the amount of total radiative forcing to be offset increases with time, and because the control gains are chosen to be constant, the overall system gain will decrease with time, meaning the system becomes increasingly stable. Therefore, we do not expect the feedback algorithm to fail for arbitrarily large amounts of injection, although the ability of the model itself to run stably or to accurately reflect the resulting climate from such large SO_2 injections is suspect. We will note that validating a model for such high levels of SO_2 injection is unlikely to occur prior to any hypothetical future deployment.

2.4. Independent Verification

The fourth step in a "well-designed" geoengineering strategy is to verify the performance of the feedback algorithm in a different, independently developed model. The purpose of this step is to demonstrate the robustness of the feedback algorithm to some sources of uncertainty. Kravitz et al. (2016) showed the importance of this in geoengineering via solar reduction, where one response had a different sign in one model than the other, but the feedback algorithm correctly compensated for any deviations to ensure that the chosen objectives were met.

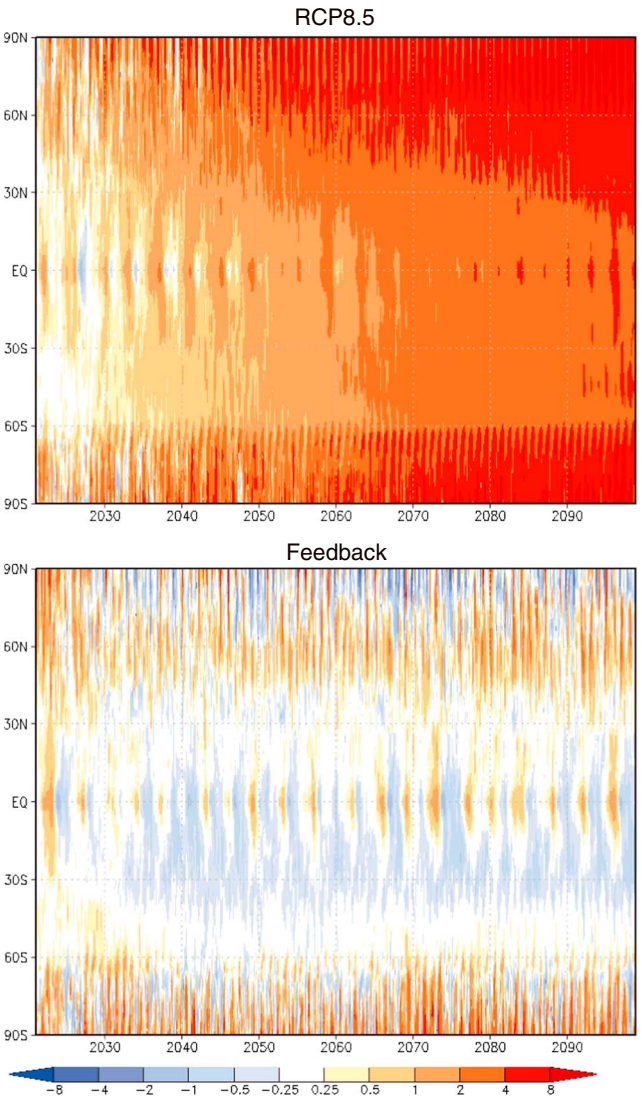

Figure 7. Zonally averaged monthly mean surface air temperature change in both the (top) RCP8.5 and (bottom) feedback simulations. Change is calculated as the difference from an average of the RCP8.5 run over years 2010–2029.

The step of independent verification is relatively straightforward for simple representations of geoengineering, such as solar reduction. This prospect is far more difficult for the representation of geoengineering investigated here, as very few models have the processes known to be important in representing stratospheric sulfate aerosol geoengineering. As such, we have not performed this step in the present study, limiting our ability to adequately assess the robustness of our geoengineering strategy. We are currently evaluating the capabilities of other models and will revisit this subject of independent verification in the future.

3. Results

We now turn to analysis of a simulation performed by employing the previously described geoengineering strategy over the period 2020–2099. All results presented below will be for the ungeoengineered RCP8.5 simulation (also called the *reference simulation* or *control simulation* by Mills et al., 2017) and the simulation in which the feedback algorithm was employed (called the *feedback simulation*).

3.1. Feedback Algorithm Performance

Figure 2 shows the performance of the feedback algorithm in meeting the three objectives, as well as the required injection (each of the four locations and the total) to meet those objectives. The algorithm results in excellent performance for all three objectives (root-mean-square departures from the baseline over the 80 years of simulation are 0.19, 0.06, and 0.04 K for T_0, T_1, and T_2, respectively).

By the last year of the simulation, meeting these objectives required an SO_2 injection rate of 51 Tg SO_2 per year in total, mostly at 30°N and 30°S. This is to some degree expected, based on knowledge obtained from solar reduction geoengineering studies: offsetting the relatively uniform forcing of CO_2 via the latitudinally distributed forcing associated with reflecting shortwave radiative flux requires greater emphasis at higher latitudes than in the tropics. The cooling is roughly linear with the amount of injection (Figure 3) for all three objectives within the injection range explored here. The regression of ΔT_1 in Figure 3 appears to be fit poorly by a single regression line. Kravitz et al. (2016) found similar behavior for solar reduction, indicating that an underlying climate process may be responsible for producing these results; they attributed these results to responses on two time scales, one less than 10 years and one greater than 10 years. Because the total time required for the first time scale to converge is approximately 10 years, this indicates a process with an *e*-folding time scale of approximately 3 years, which is consistent with land surface feedbacks. This makes sense for a variable representing hemispheric asymmetry, as the Northern Hemisphere has more land than the Southern Hemisphere. Although we are unable to robustly make the same conclusion as Kravitz et al. (2016) did for their study, our results here are consistent with that explanation: if true, T_1 would be expected to change faster early on for a given SO_2 injection, which is consistent with the steeper slope early in the simulation as seen in Figure 3.

Niemeier and Timmreck (2015) performed stratospheric sulfate aerosol geoengineering simulations using the atmosphere-only version of ECHAM5 (Giorgetta et al., 2006; Roeckner et al., 2006) coupled to the aerosol microphysical model HAM (Stier et al., 2005). This model does not have a full ocean, but it has seven aerosol modes as compared to the three modes employed in CESM1(WACCM). As such, we expect that both models can provide useful, if slightly different, representations of stratospheric sulfate aerosol geoengineering.

Niemeier and Timmreck (2015) found that the amount of top-of-atmosphere (TOA) radiative forcing is sublinear with the amount of injection. They tested out to injection amounts of 100 Tg S (approximately 200 Tg SO_2). Within the range of injections we tested, the behavior of their model is approximately linear

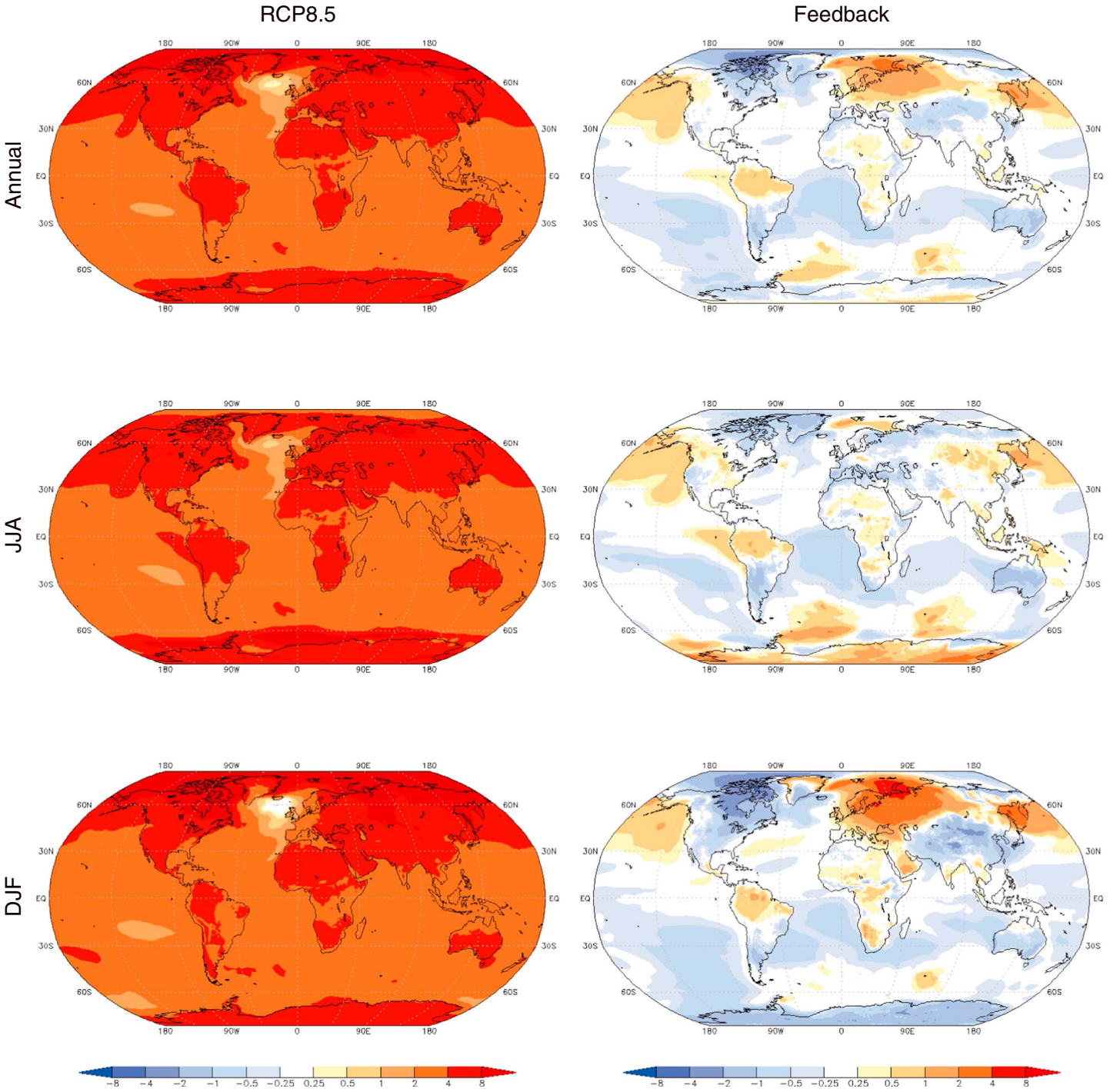

Figure 8. (top) Annual mean, (middle) JJA average, and (bottom) DJF average surface air temperature (°C) change from the baseline (2010–2029 average), averaged over the last 20 years of simulation for the (left column) RCP8.5 and (right column) feedback simulations.

with injection amount, so there is no discrepancy between their results and our Figure 3. Moreover, our results might be expected to have a greater degree of linearity than in studies involving equatorial injection because the aerosols are rapidly transported poleward, which reduces nonlinear effects due to aerosol microphysical growth (Tilmes et al., 2017).

Figure 4 shows the "forcing efficiency," which we define to be the radiative flux change for a given annual injection rate. We provide this quantity for shortwave (SW) TOA radiative flux, longwave (LW) TOA radiative flux,

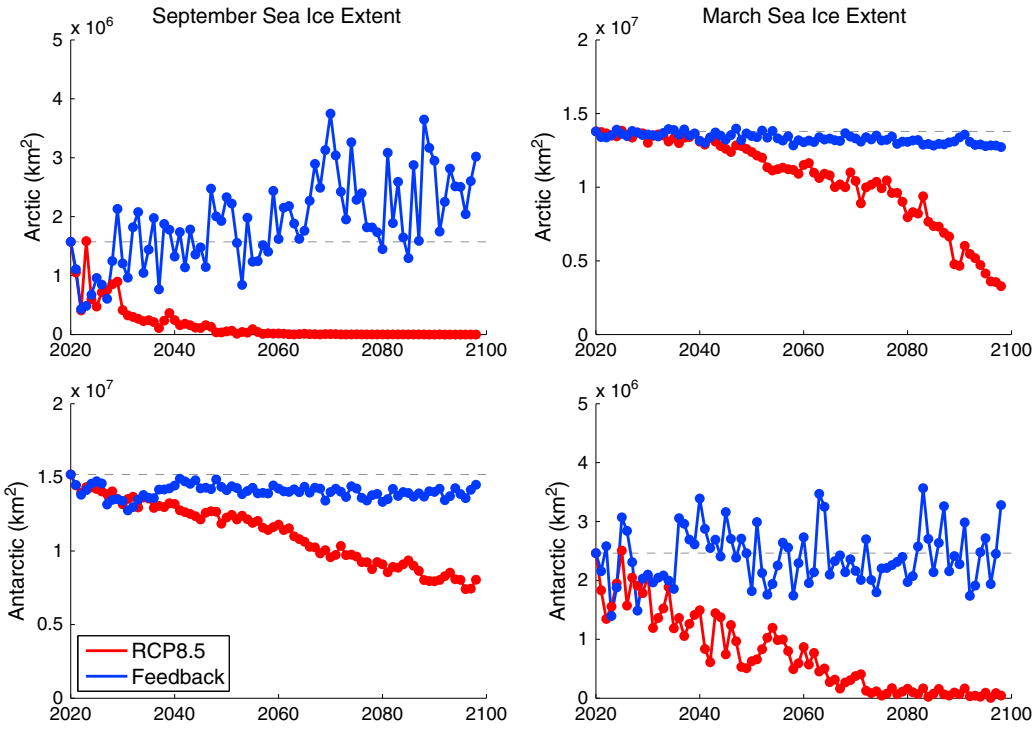

Figure 9. Maximum and minimum sea ice extent for the RCP8.5 (red) and feedback (blue) simulations. Maximum extent is defined as September sea ice extent for the Antarctic and March sea ice extent for the Arctic, and vice versa for minimum sea ice extent. Note that axes are different for minimum and maximum extent. For reference, the preindustrial (annual average) sea ice extent is 1.4×10^7 km^2 in the Arctic and 1.6×10^7 km^2 in the Antarctic (Marsh et al., 2013). In 2020, the corresponding values are 8.9×10^6 and 9.7×10^6 km^2, respectively.

and net (SW + LW) TOA radiative flux. After an initial transient period of a few years, in which the injection amounts are small and the sulfate aerosol layer accumulates mass, the efficiency shows similar results to those of Niemeier and Timmreck (2015). The efficiency magnitudes for SW and LW slightly reduce with injection amount, asymptoting toward some (as of yet) undetermined value. Within the range of injections explored here, the SW efficiency of CESM1(WACCM) is 2–3 times larger than that in ECHAM-HAM, and the LW efficiency is 5–6 times larger. The combined effect is that net efficiency is similar in the two models and remains relatively constant throughout the simulation.

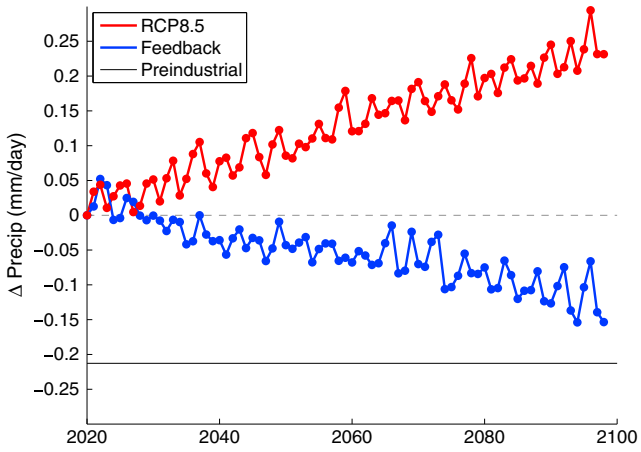

Figure 10. Annual, global mean precipitation change (mm d^{-1}) for the RCP8.5 (red) and feedback (blue) simulations. Value of 0 represents annual mean conditions in the year 2020. For reference, precipitation in the preindustrial era in CESM1(WACCM) is approximately 2.83 mm d^{-1} (black line; Marsh et al., 2013).

3.2. Aerosol Optical Depth

Figure 5 shows the time evolution of zonally averaged AOD, including the seasonal cycle. The latitudinal patterns of a peak in the midlatitudes and a tropical minimum persist throughout the simulation. Consistent with the results of Tilmes et al. (2017), AOD takes a few years at the beginning of the simulation to reach steady state. There is a notable seasonal cycle, particularly at high latitudes.

The peak value of AOD in Figure 5 is 0.83, with a global mean value of 0.52. For comparison, simulations of the 1991 eruption of Mount Pinatubo as performed by Mills et al. (2016) using a similar model indicate a peak global mean AOD of approximately 0.2.

Figure 6 shows that ℓ_0 and ℓ_2 are linear with total injection amount. After an initial adjustment period of approximately 15 years (the time it takes for the feedback loop to approximately converge given the 5 year loop time constant), the trend in ℓ_1 is negligible, and the values of ℓ_1 are negative

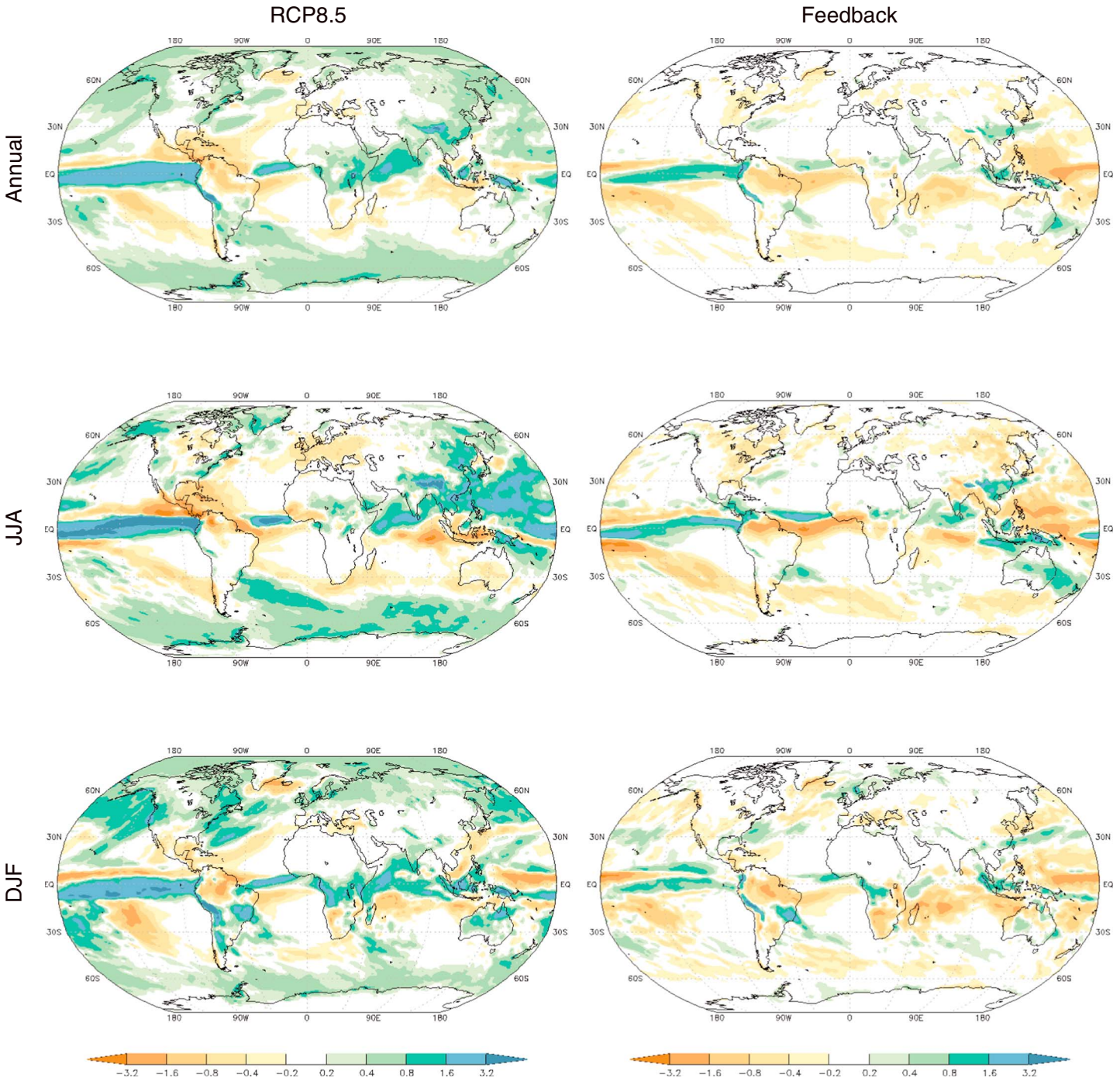

Figure 11. As in Figure 8 but for precipitation (mm d^{-1}).

(indicating more Southern Hemisphere AOD than Northern Hemisphere AOD), which is consistent with slightly greater Southern Hemisphere injection rate than a Northern Hemisphere injection rate. The results in Figure 6 indicate that the feedforward was improperly predicted prior to beginning the feedback simulation. We revisit this later in section 4.2.

3.3. Climate Effects

The three objectives chosen do not provide a holistic picture of the resulting climate effects in the feedback algorithm nor how those effects compare to results from the ungeoengineered RCP8.5 simulation.

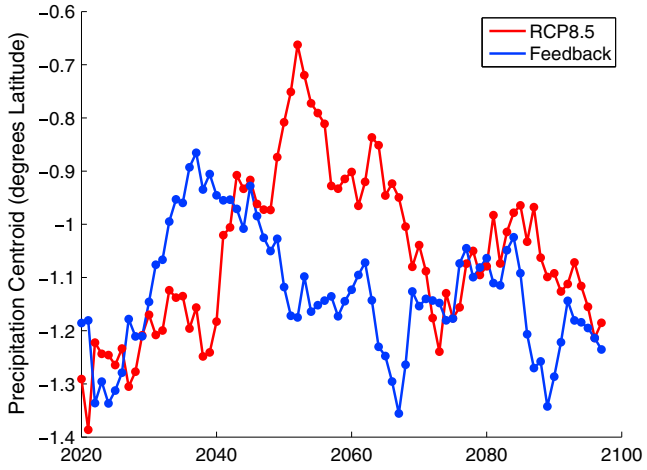

Figure 12. Five year smoothed time series of the annual mean position of the ITCZ, as defined by the centroid of global average precipitation. (See Kravitz et al. (2016) for details on the calculation.)

Figure 7 shows the time evolution of the zonally averaged surface temperature change, including the seasonal cycle. The results of the RCP8.5 simulation are consistent with known signatures of global warming (Stocker et al., 2013). Warming is amplified at high latitudes as compares to low latitudes, and the midlatitude Northern Hemisphere also warms more rapidly than the global mean, in large part due to a greater portion of land mass. Evidence of an El Niño Southern Oscillation (ENSO) persists throughout the entire simulation, but only early on do La Niña events result in tropical temperatures that are cooler than those of the baseline (blue values in Figure 7).

The feedback simulation shows that meeting the three chosen global surface temperature objectives results in relatively small surface temperature residuals at all latitudes, although a few notable residuals remain. Approximately 5% of the temperature values in the feedback simulation are statistically significantly different from the reference (2020) climate (which is what would be expected by chance), in contrast to the RCP8.5 simulation (section S1 and Figure S1 in the supporting information). Due to the immense computational expense of these simulations, we do not have additional ensemble members available that would aid in getting better quantification of the magnitude of natural variability; such simulations are planned, akin to the CESM Large Ensemble (Kay et al., 2015). The surface temperature is on average warmer than baseline in the Northern Hemisphere middle to high latitudes and in the Antarctic. Surface temperatures are cooler than the baseline in the Southern Hemisphere subtropics and in the Arctic. ENSO periodicity is unchanged from the model's natural frequency (approximately 4–5 years).

Figure 8 shows spatial features of these surface temperature differences, averaged over the last 20 years of simulation. The RCP8.5 simulation shows the same features as in Figure 7: high-latitude amplification and greater warming over land than ocean. In the feedback simulation, the Northern Hemisphere surface warming (as compared to the baseline) seen in Figure 7 is not uniform, with warming over Eurasia and the North Pacific and cooling in Northern Canada and the Arctic. These features tend to persist for both June-July-August (JJA) and December-January-February (DJF) averages, although there is some seasonal variability, namely, in the magnitude of these features. In particular, there is evidence that to achieve an objective defined for annual mean surface temperature at higher latitudes, geoengineering (as performed here) results in "overcooling" during summer and "undercooling" during winter. The explanation for this is straightforward: the aerosols only provide cooling in high latitudes in summer, whereas increased greenhouse gases warm throughout the year, but more in winter than summer. Therefore, for several months out of the year, the high latitudes are "undercooled," meaning that achieving an annual mean temperature objective at high latitudes requires "extra" cooling during the sunlit months, resulting in an "overcooling" during summer. This can be seen quite prominently in Figure 8 over the Arctic ocean, the Northern Hemispheric high latitude land masses (although with substantially more noise), and over the Antarctic continent.

Some of the high-latitude features can be explained by analyzing maximum and minimum sea ice extent (Figure 9). Whereas sea ice extent declines precipitously in the RCP8.5 simulation, it is maintained at approximately baseline levels in the feedback simulation. Antarctic minimum sea ice extent (March) reaches approximately zero by the end of the RCP8.5 simulation but remains at roughly background levels in the feedback simulation. The sea ice albedo feedback is a known contributor to Arctic amplification (e.g., Holland & Bitz, 2003), so by maintaining sea ice levels in the feedback simulation, this source of amplification of surface temperature change is suppressed. In the Arctic, September sea ice reaches zero in the RCP8.5 by approximately 2050. In the feedback simulation, September sea ice extent grows beyond its baseline value. The sea ice results are consistent with the previously described, expected result that geoengineering, to meet an annual objective, overcools in summer and undercools in winter.

The hydrological cycle will respond to changes in the total atmospheric energy budget induced by aerosol cooling. Figure 10 shows global, annual mean changes in total precipitation for the RCP8.5 and feedback simulations. The results are consistent with known effects of hydrological cycle intensification due to CO_2

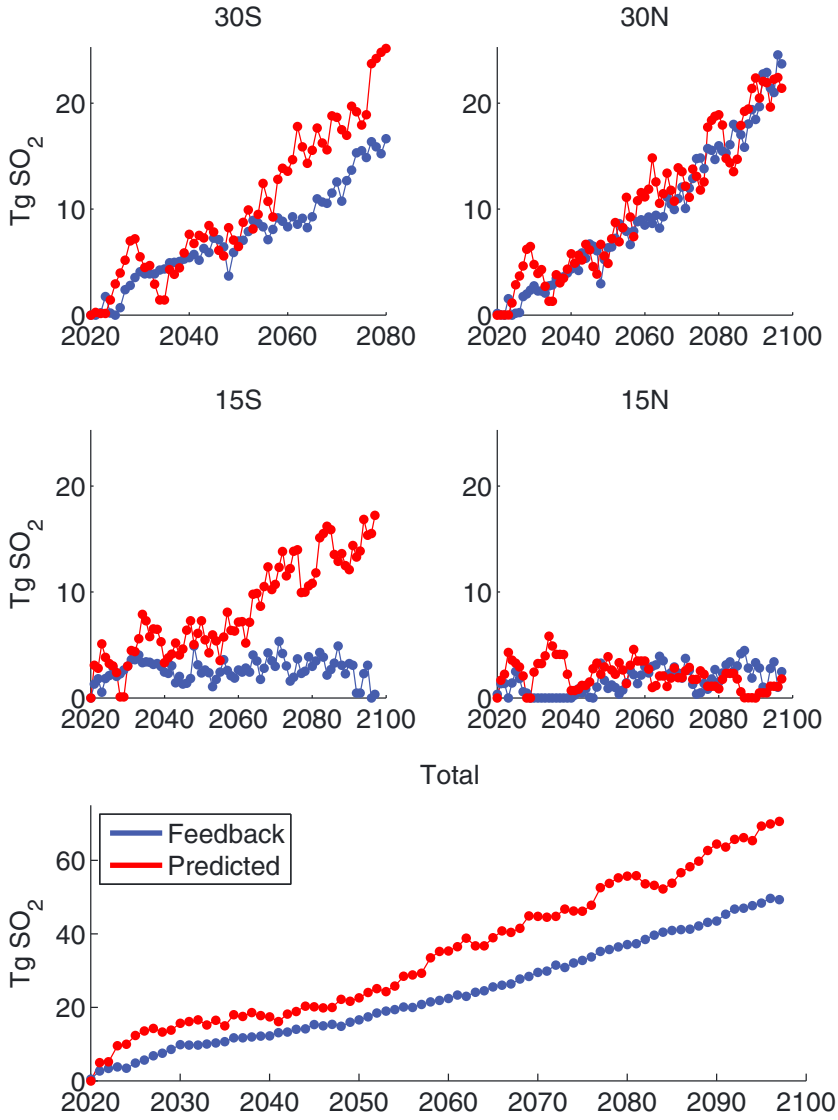

Figure 13. A comparison between the predicted required injection amounts to meet the objectives (red) and the actual required injection rates (blue). Predictions were generated based on the estimated sensitivities in Table 1 (MacMartin et al., 2017, provide further details on these calculations).

and hydrological cycle suppression under the combination of CO_2 and geoengineering forcing (e.g., Tilmes et al., 2013). In both cases, global mean precipitation stays above the preindustrial baseline. Figure 11 shows regional features of these precipitation responses, averaged over the last 20 years of simulation. (Statistical significance of these values is shown in Figure S2.) The RCP8.5 simulation features are characterized by an intensification of precipitation in many regions of the world, but particularly in the tropics and monsoon areas. As in other studies of the climate model response to geoengineering, stratospheric sulfate aerosol geoengineering tends to offset these trends (Kravitz, 2013; Tilmes et al., 2013). It is important to note that in Figure 11, both the RCP8.5 and feedback simulations show some similar features of climate response because the response in 2020 includes some climate change that has already taken place.

In the feedback simulation, the Intertropical Convergence Zone (ITCZ) is farther south than in the RCP8.5 simulation for a 25 year period (Figure 12), which is consistent with minimizing changes in T_1. (We acknowledge that this southward shift of the ITCZ has not been tested for statistical significance and may not be robust.) There is evidence for some transient behavior in the ITCZ position, indicating the potential for some disconnect between T_1 and the ITCZ position (the latter of which is better explained by cross-hemispheric energy

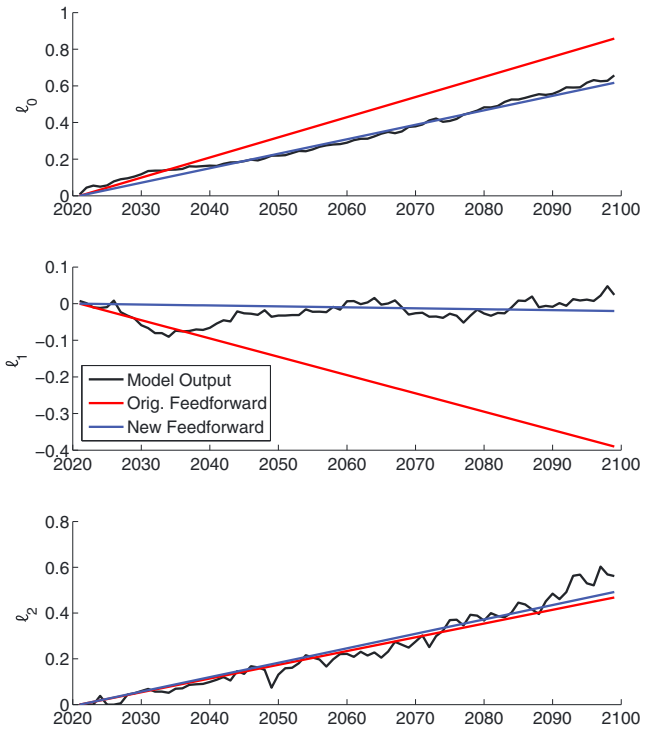

Figure 14. A comparison between the original feedforward (red) and a newly calculated feedforward (blue), which was calculated based on the results of the feedback simulation (black).

transport arguments, as described by Frierson & Hwang, 2012; Kang et al., 2008). If one wishes to include the ITCZ position as an objective, our results suggest that it would be better to control for that directly as Kravitz et al. (2016) did, rather than using T_1 as a proxy.

4. Discussion

4.1. Actual Simulation Versus Prediction

MacMartin et al. (2017) provided estimates of the coefficients G (Table 1) based on the original 10 year simulations described by Tilmes et al. (2017). By the discussions in section 2.3, we can use the time series of temperature changes in the RCP8.5 simulation to predict the required SO_2 injections at each latitude. Figure 13 shows these predictions as compared to the actual injection rates determined by the feedback algorithm.

The Northern Hemisphere injection rates are quite well predicted, but the predicted Southern Hemisphere injection rates are substantially higher than the actual injection rates. In particular, the predicted amount of injection at 15°S steadily increased throughout the simulation, and very little was actually called for by the feedback algorithm.

The explanation for this difference in the Southern Hemisphere can be explained by an understanding of time scales of feedbacks in the Southern Ocean. The predictions were generated based on the climate system response to a 10 year simulation, which is an insufficient time to get appreciable cooling over a large oceanic region like the Southern Ocean. This result is explained by MacMartin et al. (2017), who show comparatively little cooling in the Southern Ocean for injections at 15°S or 30°S. Using these computed sensitivities would result in a prediction that cooling the Southern Ocean would require a large amount of injection into the Southern Hemisphere, much more so than the required Northern Hemisphere injection to reduce Northern Hemisphere temperature.

This comparatively low sensitivity is true for time scales up to 10 years, but after that initial time period, the climate response is dominated by ocean time scales, so the sensitivities of the two hemispheres would be similar. Indeed, this is how the feedback algorithm results play out: for the first couple of decades, the algorithm calls for Southern Hemisphere injections that are consistent with those predicted, but afterward, the required injections in the Southern Hemisphere are substantially less than what was predicted and are similar in magnitude to the Northern Hemisphere injections.

4.2. Feedforward Improvements

Based on the results in section 4.1, our feedforward was too aggressive. From the results of the simulation, we can retrospectively calculate a better feedforward. To calculate the correct sensitivities, we perform linear regression on the AOD (ℓ_0, ℓ_1, and ℓ_2) required in the feedback simulation (Figure 14). The new feedforward design is $\hat{\ell}_0 = 0.0079(t - t_{\text{ref}})$, $\hat{\ell}_1 = -2.5758 \times 10^{-4}(t - t_{\text{ref}})$, and $\hat{\ell}_2 = 0.0063(t - t_{\text{ref}})$. Figure 14 shows that the new ℓ_0 and ℓ_1 feedforwards are smaller in magnitude than the original ones. This is due to the feedforwards being estimated on 10 years of simulation, which was insufficient to capture the longer-term dynamics, particularly for estimating ℓ_1. Our original estimate for ℓ_2 was quite accurate. As was discussed previously, linear regression is an overly simplistic choice for designing a feedforward, and a more accurate method would be to use a low-order dynamic model of the climate system response to sulfate AOD (MacMartin, Caldeira, et al., 2014).

5. Conclusions

Here we have demonstrated that despite all of the complexities and nonlinearities associated with stratospheric sulfate aerosol geoengineering, we were able to use feedback to meet three simultaneous temperature objectives in the presence of climate response uncertainty in a state-of-the-art Earth System Model. We accomplished this by annually adjusting the amount of stratospheric SO_2 injection at four locations: primarily 30°N/S and a smaller amount at 15°N/S. This represents the first time that controllability of stratospheric

sulfate aerosol geoengineering to meet global climate objectives has been demonstrated, albeit in a limited sense. This demonstration was conducted using a climate model that is currently our best representation of the climate system behaviors that are necessary to simulate stratospheric sulfate aerosol geoengineering.

Designing the actual feedback algorithm required results from system identification simulations, but these calculations were also aided by previous work involving solar irradiance reduction (Kravitz et al., 2016). While solar irradiance reduction does not capture many of the relevant processes in sulfate aerosol geoengineering, it provides enough information about the broad radiative effects of solar geoengineering in general so as to be useful in this regard. Moreover, because solar irradiance reduction is easy to simulate and can be performed in cheaper models than CESM1(WACCM), it lends itself well to model intercomparisons to better understand intermodel robustness of results from geoengineering (Kravitz, 2013; Kravitz et al., 2011). We stress the importance of a complementary approach using both simple and complex methods of representing geoengineering in climate models in any future research endeavors.

While this study was a crucial step in exploring the space of achievable climates through geoengineering, there are a number of caveats and future directions of research. Here we explored the ability of four selected degrees of freedom (the four latitudes of SO_2 injection) in stratospheric sulfate aerosol geoengineering to meet three global surface temperature objectives. Controlling for temperature residuals, as seen in Figure 8, or for other variables, such as the ones shown in section 3.3, may require additional *independent* degrees of freedom. This could include different latitudes or altitudes of injection, expanding the space of the already explored degrees of freedom. It could also include injecting in different seasons to achieve regional or seasonally varying objectives, such as adjusting Indian monsoon precipitation (MacMartin et al., 2013). Another potential degree of freedom is aerosol composition: different aerosols have different climate effects, which may be advantageous for meeting chosen objectives or might affect the severity of unintended side effects (Ferraro et al., 2015b; Keith et al., 2016; Weisenstein et al., 2015). Even among all of these potential degrees of freedom, there may be objectives that stratospheric sulfate aerosol geoengineering is incapable of meeting. In this case, different forms of geoengineering, such as marine cloud brightening (Latham, 1990), might be able to complement stratospheric sulfate aerosol geoengineering to meet additional objectives.

We will note that none of the residuals in Figures 8 and 11 was statistically significant. This implies a need for defining "tolerance limits" when establishing objectives of geoengineering. What range of performance of the feedback strategy is "good enough"? This is ultimately a subjective choice and will be limited by detectability, as for finer thresholds of tolerance, one may need larger observation times to ensure the desired performance of the geoengineering strategy (MacMynowski et al., 2011). Progress continues to be made on detection and attribution of geoengineering (Bürger & Cubasch, 2015; Lo et al., 2016), which may aid in this discussion of tolerance limits.

Of key importance here is linearity: interactions between the various degrees of freedom could affect the space of achievable climates. Tilmes et al. (2017) and MacMartin et al. (2017) gave an indication of the process required for system identification to determine the climate effects, including nonlinear effects, from modifying the degrees of freedom explored here. Fully characterizing the geoengineering parameter space would require a great expansion of these effects and would likely include multiple models to assess the range of intermodel uncertainty in characterizing the response. Also, as was revealed in section 4.1, 10 years of simulation is insufficient for characterizing all of the relevant dynamics in the work presented here. Any future effort would need to consider what dynamics are necessary to represent and conduct system identification simulations accordingly.

The issue of multiple models brings up the importance of independent verification of the feedback algorithm (section 2.4), which we did not undertake here. To ascertain robustness of the feedback algorithm, it is insufficient to test the algorithm in the same model that was used to design it. Independently verifying the algorithm's performance in a separate climate model is a crucial confidence-building step that the algorithm is robust to some degree of uncertainty in the climate system response to both climate change and geoengineering. Kravitz et al. (2014, 2016) used two state-of-the-art Earth System Models (ESMs) to design and verify a feedback algorithm that operated on solar irradiance reduction, a process that every ESM can represent. Determining which model to use for independent verification for the more complicated case of stratospheric sulfate aerosols would require some care in both implementation and interpreting the results, as some of the intermodel variations in response may be due to differences in which processes (especially stratospheric aerosol processes) are represented by the two models.

Although the version of CESM1(WACCM) that we used is well validated against observations of volcanic eruptions, the aerosol microphysics representation may not be well suited to properly represent some of the most important nonlinearities associated with stratospheric sulfate aerosol growth. The version of the model we used employs the Modal Aerosol Model (MAM; Liu et al., 2012) with three logarithmically distributed aerosol modes that have fixed distribution widths. A more complex representation would be to replace MAM with the Community Aerosol and Radiation Model for Atmospheres (CARMA; Toon et al., 1988), which has been successfully implemented in WACCM (English et al., 2011). CARMA is a sectional model that represents aerosol nucleation, growth, evaporation, sedimentation, and coagulation, and can be configured to resolve sulfate aerosol size using more than 30 size bins. Its performance has been validated against in situ observations of stratospheric sulfate aerosol from volcanic and other background sources (Campbell et al., 2014). English et al. (2012) used WACCM/CARMA to simulate stratospheric sulfate aerosol geoengineering and found results that suggest this more complicated treatment may be warranted in particular circumstances. This additional granularity comes at greatly increased computational expense, so any explorations with CARMA would need to be judicious to determine situations in which this more thorough treatment is necessary for representing aerosol microphysical growth. The importance of using CARMA could preliminarily be determined by simulating a small set of conditions.

The feedback algorithm employed here used proportional-integral control, which is the same algorithmic structure as that used by MacMartin, Kravitz, et al. (2014) and Kravitz et al. (2014, 2016). While simple and effective for the problems investigated here and in those previous studies, it may be insufficient for more complicated objectives, such as regionally or seasonally varying targets. Meeting those objectives could require more advanced tools from control theory than have been explored here. In addition, the feedforward implemented here was a simple linear approximation of the temperature change based on an already conducted RCP8.5 run. In a real-world scenario, the future trajectory of climate change, and hence the estimated amount of injection required going forward, is unknown. Such a situation could benefit from a Model Predictive Control or receding horizons approach whereby the feedforward form is adjusted at the update rate based on updated information about expected future climate change (e.g., Jarvis & Leedal, 2012; MacMartin, Caldeira, et al., 2014).

The results we obtained in this study have benefits for practical and engineering research on geoengineering. One of the difficulties of stratospheric aerosol geoengineering is transporting the material to a high altitude (McClellan et al., 2012). As MacMartin et al. (2017) discuss, using subtropical injection is better at meeting the particular chosen objectives than using purely tropical injection. Furthermore, the present study indicates that the chosen objectives could be met using mostly injection at 30° in latitude, where the tropopause is substantially lower than at the equator, implying that the injection height of material could be lower than was previously thought. Of course, different objectives may have different criteria for injection locations.

The results presented here are a necessary step toward understanding the potential role geoengineering may play in addressing climate change, in particular, understanding what geoengineering can do and what it cannot do.

Acknowledgments
This research was developed with funding from the Defense Advanced Research Projects Agency (DARPA). The views, opinions, and/or findings expressed are those of the authors and should not be interpreted as representing the official views or policies of the Department of Defense or the U.S. Government. The Pacific Northwest National Laboratory is operated for the U.S. Department of Energy by Battelle Memorial Institute under contract DE-AC05-76RL01830. Simulations were carried out on the Yellowstone high-performance computer platform (Computational and Informational Systems Laboratory 2012). The CESM project is supported by the National Science Foundation and the Office of Science (BER) of the U.S. Department of Energy. The National Center for Atmospheric Research is funded by the National Science Foundation. Model output for the 10 year system identification simulations (Tilmes et al., 2017) is available on the Earth System Grid at https://doi.org/10.5065/D6X63KMM.

References

Ban-Weiss, G. A., & Caldeira, K. (2010). Geoengineering as an optimization problem. *Environmental Research Letters*, *5*, 031001.

Berdahl, M., Robock, A., Ji, D., Jones, A., Kravitz, B., Moore, J. C., & Watanabe, S. (2014). Arctic cryosphere response in the geoengineering model intercomparison project (GeoMIP) G3 and G4 scenarios. *Journal of Geophysical Research: Atmospheres*, *119*, 1308–1321. https://doi.org/10.1002/2013JD020627

Budyko, M. I. (1974). *Climate and life*. London: Academic Press.

Bürger, G., & Cubasch, U. (2015). The detectability of climate engineering. *Journal of Geophysical Research: Atmospheres*, *120*, 11,404–11,418. https://doi.org/10.1002/2015JD023954

Campbell, P., Mills, M. J., & Deshler, T. (2014). The global extent of the mid stratospheric CN layer: A three-dimensional modeling study. *Journal of Geophysical Research: Atmospheres*, *119*, 1015–1030. https://doi.org/10.1002/2013JD020503

Crutzen, P. J. (2006). Albedo enhancement by stratospheric sulfur injections: A contribution to resolve a policy dilemma? *Climatic Change*, *77*, 211–220.

Curry, C. L., Sillmann, J., Bronaugh, D., Alterskjær, K., Cole, J. N. S., Kravitz., B., … Tilmes, S. (2014). A multi-model examination of climate extremes in an idealized geoengineering experiment. *Journal of Geophysical Research: Atmospheres*, *119*, 3900–3923. https://doi.org/10.1002/2013JD020648

English, J. M., Toon, O. B., & Mills, M. J. (2012). Microphysical simulations of sulfur burdens from stratospheric sulfur geoengineering. *Atmospheric Chemistry and Physics*, *12*, 4775–4793.

English, J. M., Toon, O. B., Mills, M. J., & Yu, F. (2011). Microphysical simulations of new particle formation in the upper troposphere and lower stratosphere. *Atmospheric Chemistry and Physics*, *11*, 9303–9322.

Ferraro, A. J., Charlton-Perez, A. J., & Highwood, E. J. (2015a). A risk-based framework for assessing the effectiveness of stratospheric aerosol geoengineering. *PLoS One*, *9*, e88849.

Ferraro, A. J., Charlton-Perez, A. J., & Highwood, E. J. (2015b). Stratospheric dynamics and midlatitude jets under geoengineering with space mirrors and sulfate and titania aerosols. *Journal of Geophysical Research: Atmospheres*, *120*, 414–429. https://doi.org/10.1002/2014JD022734

Ferraro, A. J., Highwood, E. J., & Charlton-Perez, A. J. (2011). Stratospheric heating by potential geoengineering aerosols. *Geophysical Research Letters*, *38*, L24706. https://doi.org/10.1029/2011GL049761

Frierson, D. M. W., & Hwang, Y.-T. (2012). Extratropical influence on ITCZ shifts in slab ocean simulations of global warming. *Journal of Climate*, *25*, 720–733.

Giorgetta, M. A., Manzini, E., Roeckner, E., Esch, M., & Bengtsson, L. (2006). Climatology and forcing of the quasi-biennial oscillation in the MAECHAM5 model. *Journal of Climate*, *19*, 3882–3901.

Glienke, S., Irvine, P. J., & Lawrence, M. G. (2015). The impact of geoengineering on vegetation in experiment G1 of the GeoMIP. *Journal of Geophysical Research: Atmospheres*, *120*, 10,196–10,213. https://doi.org/10.1002/2015JD024202

Hansen, J., Sato, M., & Ruedy, R. (1997). Radiative forcing and climate response. *Journal of Geophysical Research*, *102*, 6831–6864.

Haywood, J. M., Jones, A., Dunstone, N., Milton, S., Vellinga, M., Bodas-Salcedo, A., … Stephens, G. (2016). The impact of equilibrating hemispheric albedos on tropical performance in the HadGEM2-ES coupled climate model. *Geophysical Research Letters*, *43*, 395–403. https://doi.org/10.1002/2015GL066903

Heckendorn, P., Weisenstein, D., Fueglistaler, S., Luo, B. P., Rozanov, E., Schraner, M., … Peter, T. (2009). The impact of geoengineering aerosols on stratospheric temperature and ozone. *Environmental Research Letters*, *4*, 045108.

Holland, M. M., & Bitz, C. M. (2003). Polar amplification of climate change in coupled models. *Climate Dynamics*, *21*, 221–232.

Hurrell, J. W., Holland, M. M, Gent, P. R., Ghan, S., Kay, J. E., Kushner, P. J., … Marshall, S. (2013). The Community Earth System Model: A framework for collaborative research. *Bulletin of the American Meteorological Society*, *94*, 1339–1360.

Jackson, L. S., Crook, J. A., Jarvis, A., Leedal, D., Ridgwell, A., Vaughan, N., & Forster, P. M. (2015). Assessing the controllability of arctic sea ice extent by sulfate aerosol geoengineering. *Geophysical Research Letters*, *42*, 1223–1231. https://doi.org/10.1002/2014GL062240

Jarvis, A., & Leedal, D. (2012). The Geoengineering Model Intercomparison Project (GeoMIP): A control perspective. *Atmospheric Science Letters*, *13*, 157–163.

Kalidindi, S., Bala, G., Modak, A., & Caldeira, K. (2014). Modeling of solar radiation management: A comparison of simulations using reduced solar constant and stratospheric sulfate aerosols. *Climate Dynamics*, *44*, 2909–2925.

Kang, S. M., Held, I. M., Frierson, D. W., & Zhao, M. (2008). The response of the ITCZ to extratropical thermal forcing: Idealized slab-ocean experiments with a GCM. *Journal of Climate*, *21*, 3521–3532.

Kay, J. E., Deser, C., Phillips, A., Mai, A., Hannay, C., Strand, G, … Vertenstein, M. (2015). The Community Earth System Model (CESM) large ensemble project: A community resource for studying climate change in the presence of internal climate variability. *Bulletin of the American Meteorological Society*, *96*, 1333–1349.

Keith, D. W., Weisenstein, D. K., Dykema, J. A., & Keutsch, F. N. (2016). Stratospheric solar geoengineering without ozone loss? *Proceedings of the National academy of Sciences*, *113*, 14,910–14,914.

Kravitz, B. (2013). *Climate engineering with stratospheric aerosols and associated engineering parameters*, paper presented at Frontiers of engineering: Reports on leading-edge engineering from the 2012 symposium, National Academy of Engineering,Washington, DC: National Academies Press.

Kravitz, B., Caldeira, K., Boucher, O., Robock, A., Rasch, P. J., Alterskjær, K., … Yoon, J.-H. (2013). Climate model response from the Geoengineering Model Intercomparison Project (GeoMIP). *Journal of Geophysical Research: Atmospheres*, *118*, 8320–8332. https://doi.org/10.1002/jgrd.50646

Kravitz, B., MacMartin, D. G., Leedal, D. T., Rasch, P. J., & Jarvis, A. J. (2014). Explicit feedback and the management of uncertainty in meeting climate objectives with solar geoengineering. *Environmental Research Letters*, *9*, 044006.

Kravitz, B., MacMartin, D. G., Wang, H., & Rasch, P. J. (2016). Geoengineering as a design problem. *Earth System Dynamics*, *7*, 469–497.

Kravitz, B., Robock, A., Boucher, O., Schmidt, H., Taylor, K. E., Stenchikov, G., & Schulz, M. (2011). The geoengineering model intercomparison project (GeoMIP). *Atmospheric Science Letters*, *12*, 162–167.

Latham, J. (1990). Control of global warming? *Nature*, *347*, 339–340.

Liu, X., et al. (2012). Toward a minimal representation of aerosols in climate models: Description and evaluation in the Community Atmosphere Model CAM5. *Geoscientific Model Development*, *5*, 709–739.

Lo, Y. T. E., Charlton-Perez, A. J., Lott, F. C., & Highwood, E. J. (2016). Detecting sulphate aerosol geoengineering with different methods. *Nature Scientific Reports*, *6*, 39169.

MacMartin, D. G., Caldeira, K., & Keith, D. W. (2014). Solar geoengineering to limit the rate of temperature change. *Philosophical Transactions of the Royal Society A*, *372*, 20140134.

MacMartin, D. G., Keith, D. W., Kravitz, B., & Caldeira, K. (2013). Management of trade-offs in geoengineering through optimal choice of non-uniform radiative forcing. *Nature Climate Change*, *3*, 365–368.

MacMartin, D. G., Kravitz, B., Keith, D. W., & Jarvis, A. (2014). Dynamics of the coupled human-climate system resulting from closed-loop control of solar geoengineering. *Climate Dynamics*, *43*, 243–258.

MacMartin, D. G., Kravitz, B., Long, J. C. S., & Rasch, P. J. (2016). Geoengineering with stratospheric aerosols: What don't we know after a decade of research? *Earth's Future*, *4*, 543–548.

MacMartin, D. G., Kravitz, B., Tilmes, S., Richter, J. H., Mills, M. J., Jean-Francois, L., … Vitt, F. (2017). The climate response to stratospheric aerosol geoengineering can be tailored using multiple injection locations. *Journal of Geophysical Research: Atmospheres*, *122*. https://doi.org/10.1002/2017JD026868

MacMynowski, D. G., Keith, D. W., Caldeira, K., & Shin, H.-J. (2011). Can we test geoengineering? *Energy and Environmental Science*, *4*, 5044.

Marsh, D. R., Mills, M. J., Kinnison, D. E., Lamarque, J.-F., Calvo, N., & Polvani, L. M. (2013). Climate change from 1850 to 2005 simulated in CESM1(WACCM). *Journal of Climate*, *26*, 7372–7391.

McClellan, J., Keith, D. W., & Apt, J. (2012). Cost analysis of stratospheric albedo modification delivery systems. *Environmental Research Letters*, *7*, 034019.

Meinshausen, M., Smith, S. J., Calvin, K., Daniel, J. S., Kainuma, M. L. T., Lamarque, J-F., … van Vuuren, D. P. (2011). The RCP greenhouse gas concentrations and their extensions from 1765 to 2300. *Climatic Change*, *109*, 213.

Mills, M. J., Richter, J. H., Tilmes, S., Kravitz, B., MacMartin, D. G., Glanville, A. A., … Kinnison, D. E. (2017). Radiative and chemical response to interactive stratospheric sulfate aerosols in fully coupled CESM1(WACCM). *Journal of Geophysical Research: Atmospheres*, *122*. https://doi.org/10.1002/2017JD027006

Mills, M. J., Schmidt, A., Easter, R., Solomon, S., Kinnison, D. E., Ghan, S. J., … Gettelman, A. (2016). Global volcanic aerosol properties derived from emissions, 1990–2014, using CESM1(WACCM). *Journal of Geophysical Research: Atmospheres*, *121*, 2332–2348. https://doi.org/10.1002/2015JD024290

Moore, J. C., Rinke, A., Yu, X., Ji, D., Cui, X., Li, Y., … Watanabe, S. (2014). Arctic sea ice and atmospheric circulation under the GeoMIP G1 scenario. *Journal of Geophysical Research: Atmospheres*, *119*, 567–583. https://doi.org/10.1002/2013JD021060

Moss, R. H., Moss, R. H., Edmonds, J. A., Hibbard, K. A., Manning, M. R., Rose, S. K., … Wilbanks T. J. (2010). The next generation of climate scenarios. *Nature*, *463*, 747–756.

National Research Council (NRC) (2015). Climate intervention: Reflecting sunlight to cool earth. Retrieved from http://www.nap.edu/catalog/18988/climate-intervention-reflecting-sunlig%ht-to-cool-earth, last Access: 7 May 2015.

Niemeier, U., & Timmreck, C. (2015). What is the limit of climate engineering by stratospheric injection of SO_2? *Atmospheric Chemistry and Physics*, *15*, 9129–9141.

Niemeier, U., Schmidt, H., Alterskjær, K., & Kristjánsson, J. E. (2013). Solar irradiance reduction via climate engineering: Impact of different techniques on the energy balance and the hydrological cycle. *Journal of Geophysical Research: Atmospheres*, *118*, 11,905–11,917. https://doi.org/10.1002/2013JD020445

Pitari, G., Aquila, V., Kravitz, B., Robock, A., Watanabe, S., Luca, N. D., … Cionni, I. (2014). Stratospheric ozone response to sulfate geoengineering: Results from the Geoengineering Model Intercomparison Project (GeoMIP). *Journal of Geophysical Research: Atmospheres*, *119*, 2629–2653. https://doi.org/10.1002/2013JD020566

Richter, J. H., Tilmes, S., Mills, M. J., Tribbia, J., Kravitz, B., MacMartin, D. G., … Jean-Francois, L. (2017). Stratospheric dynamical response and ozone feedbacks in the presence of SO_2 injections. *Journal of Geophysical Research: Atmospheres*, *122*. https://doi.org/10.1002/2017JD026912

Robock, A. (2000). Volcanic eruptions and climate. *Reviews of Geophysics*, *38*, 191–219.

Robock, A., Oman, L., & Stenchikov, G. L. (2008). Regional climate responses to geoengineering with tropical and Arctic SO_2 injections. *Journal of Geophysical Research*, *113*, D16101. https://doi.org/10.1002/2013JD020566

Roeckner, E., Brokopf, R., Esch, M., Giorgetta, M., Hagemann, S., Kornblueh, L., … Schulzweida, U. (2006). Sensitivity of simulated climate to horizontal and vertical resolution in the ECHAM5 atmosphere model. *Journal of Climate*, *19*, 3771–3791.

Stier, P., Feichter, J., Kinne, S., Kloster, S., Vignati, E., Wilson, J., … Petzold, A. (2005). The aerosol-climate model ECHAM5-HAM. *Atmospheric Chemistry and Physics*, *5*, 1125–1156.

Stocker, T. F., Qin, D., Plattner, G.-K., Alexander, L. V., Allen, S. K., Bindoff, N. L., … Xie, S.-P. (2013). Technical summary. In T. F. Stocker et al. (Eds.), *Climate change 2013: The physical science basis. Contribution of Working Group I to the Fifth Assessment Report of the Intergovernmental Panel on Climate Change*. Cambridge, UK: Cambridge University Press.

Tilmes, S., Fasullo, J., Lamarque, J.-F., Marsh, D. R., Mills, M., Alterskjær, K., … Watanabe, S. (2013). The hydrological impact of geoengineering in the Geoengineering Model Intercomparison Project (GeoMIP). *Journal of Geophysical Research: Atmospheres*, *118*, 11,036–11,058. https://doi.org/10.1002/jgrd.50868

Tilmes, S., Garcia, R. R., Kinnison, D. E., Gettelman, A., & Rasch, P. J. (2009). Impact of geoengineered aerosols on the troposphere and stratosphere. *Journal of Geophysical Research*, *114*, D12305. https://doi.org/10.1029/2008JD011420

Tilmes, S., Richter, J. H., Mills, M. J., Kravitz, B., MacMartin, D. G., Vitt, F., … Lamarque, J.-F. (2017). Sensitivity of aerosol distribution and climate response to stratospheric$_2$ injection locations. *Journal of Geophysical Research: Atmospheres*, *122*. https://doi.org/10.1002/2017JD026888

Tilmes, S., Sanderson, B. M., & O'Neill, B. C. (2016). Climate impacts of geoengineering in a delayed mitigation scenario. *Geophysical Research Letters*, *43*, 8222–8229. https://doi.org/10.1002/2016GL070122

Toon, O. B., Turco, R. P., Westphal, D. L., Malone, R., & Liu, M. S. (1988). A multidimensional model for aerosols: Description of computational analogs. *Journal of Atmospheric Sciences*, *45*, 2123–2144.

Weisenstein, D. K., Keith, D. W., & Dykema, J. A. (2015). Solar geoengineering using solid aerosol in the stratosphere. *Atmospheric Chemistry and Physics*, *15*, 11,835–11,859.

Xia, L., Robock, A., Cole, J. N. S., Curry, C. L., Ji, D., Jones, A., … Yoon, J.-H. (2014). Solar radiation management impacts on agriculture in China: A case study in the Geoengineering Model Intercomparison Project (GeoMIP). *Journal of Geophysical Research: Atmospheres*, *119*, 8695–8711. https://doi.org/10.1002/2013JD020630